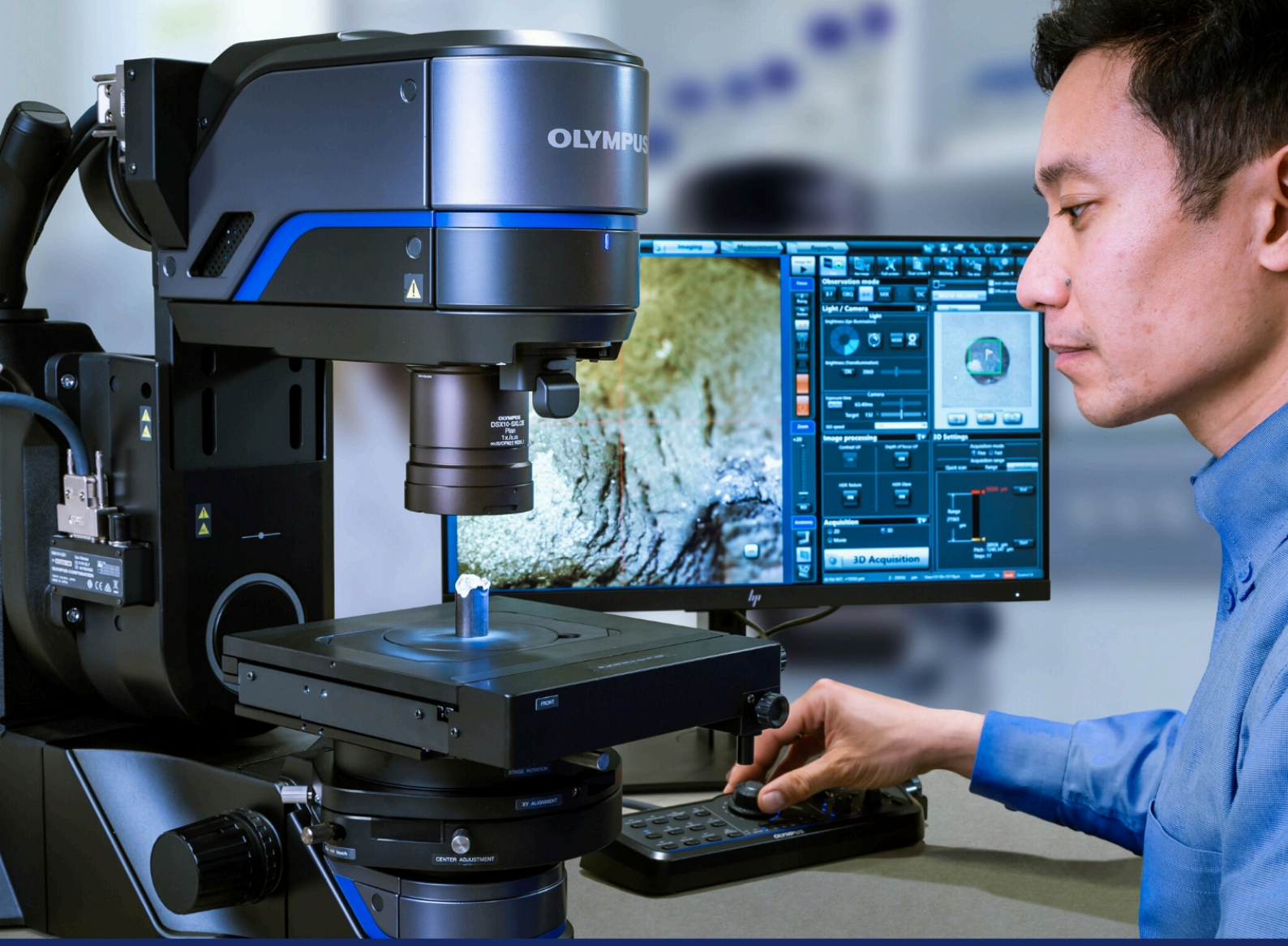

Science Meets Technology with Advanced Optical Metrology

Access in-depth information on methods and applications in the R&D field of optical metrology through free to access article digests of recent peer-reviewed publications and more.

Discover advancedopticalmetrology.com now!

OLYMPUS

WILEY

ADVANCED ENERGY MATERIALS
www.advenergymat.de

Work Function Evolution in Li Anode Processing

Ane Etxebarria, Stephan L. Koch, Oleksandr Bondarchuk, Stefano Passerini, Gilberto Teobaldi,* and Miguel Ángel Muñoz-Márquez**

Toward improved understanding and control of the interactions of Li metal anodes with their processing environments, a combined X-ray photoelectron spectroscopy (XPS), ultraviolet photoelectron spectroscopy (UPS), and density functional theory (DFT) characterization of the effects that O_2, CO_2, and N_2, the main gases in dry-atmosphere battery production lines, induced on a reproducibly clean Li surface at room temperature is presented here. XPS measurements demonstrate that O_2 is ten times more effective than CO_2 at oxidizing metal Li. Notably, pure N_2 is shown to not dissociate on clean metal Li. UPS results indicate that decomposition of O_2 (CO_2) reduces the work function of the Li surface by almost 1 eV, therefore increasing the reduction energy drive for the treated substrate by comparison to bare metallic Li. DFT simulations semiquantitatively account for these results on the basis of the effects of dissociative gas adsorption on the surface dipole density of the Li surface.

1. Introduction

Practical realization of next-generation energy storage systems, such as Li–metal, Li–S, and Li–O_2 batteries, rests on the availability of stable Li metal anodes.[1] For progress in any of these, expectedly transformative, battery technologies to accelerate and reach market point, advances in the handling and processing of metallic lithium are needed. Such advances can only be made possible by accurate fundamental understanding and control of the interactions of Li metal with its surroundings, starting from, but not limited to, Li processing environments. Unfortunately, such understanding and control is disappointingly poor due to the unsolved challenges in obtaining pure metallic Li surfaces. These unsolved challenges in turn result in either a lack of quantitatively resolved experiments on pure metallic Li surfaces or, for the few experiments available, stark contrasts in their interpretation, which we detail below (Section 2.1).[2–18] Although important progress has been made in dealing with commercial Li metal samples, such progress has been invariably made by means of advanced electrolytes,[19,20] mechanical surface modifications,[21] and other surface engineering methods such as application of coatings, that is, avoiding to directly tackle the challenges associated with processing of pristine metal Li substrates.[22–25]

Perhaps surprisingly, yet undeniably, academic advances in electrochemical cycling of Li metal anodes to date[19–24] have been made without quantitative characterization and knowledge of the composition (read contamination) and electronic properties of the pristine lithium surfaces, which will eventually react to form interfaces with the electrolytes. Such a lack of quantitative knowledge on the pristine Li anode inevitably hinders effective development of strategies to its stabilization. As a result, commercially viable metal Li anodes are yet to be

A. Etxebarria, Dr. O. Bondarchuk,[+] Dr. M. A. Muñoz-Márquez
Centre for Cooperative Research on Alternative Energies (CIC energiGUNE)
Basque Research and Technology Alliance (BRTA)
Alava Technology Park, Albert Einstein 48, Vitoria-Gasteiz 01510, Spain
E-mail: mamunoz@cicenergigune.com

A. Etxebarria
Departamento de Física de la Materia Condensada
Facultad de Ciencia y Tecnología, Universidad del País Vasco (UPV/EHU)
P.O. Box 644, Bilbao 48080, Spain

The ORCID identification number(s) for the author(s) of this article can be found under https://doi.org/10.1002/aenm.202000520.

[+]Present address: International Iberian Nanotechnology Laboratory, Av. Mestre José Veiga, Braga 4715-330, Portugal

DOI: 10.1002/aenm.202000520

Dr. S. L. Koch, Prof. S. Passerini
Helmholtz Institute Ulm (HIU)
Helmholtzstrasse 11, Ulm 89081, Germany
E-mail: stefano.passerini@kit.edu

Dr. S. L. Koch, Prof. S. Passerini
Karlsruhe Institute of Technology (KIT)
P.O. Box 3640, Karlsruhe 76021, Germany

Dr. G. Teobaldi
Scientific Computing Department
STFC UKRI
Rutherford Appleton Laboratory
Harwell Campus, Didcot OX11 0QX, UK
E-mail: gilberto.teobaldi@stfc.ac.uk

Dr. G. Teobaldi
Stephenson Institute for Renewable Energy
Department of Chemistry
University of Liverpool
Liverpool L69 3BX, UK

Dr. G. Teobaldi
School of Chemistry
University of Southampton
Highfield, Southampton SO17 1BJ, UK

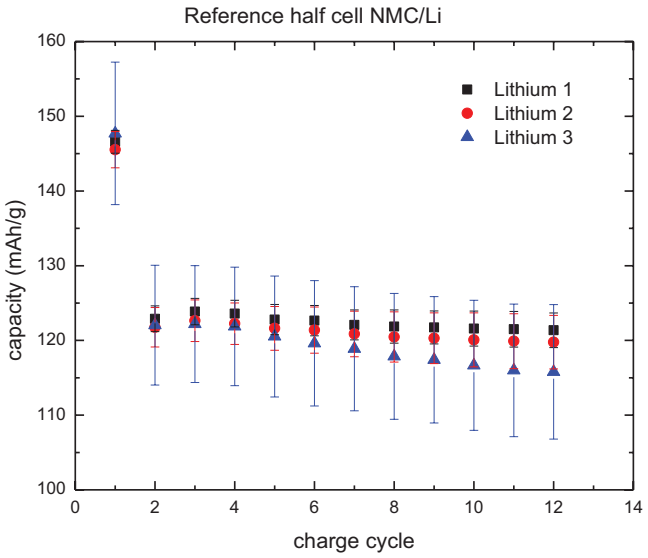

Figure 1. Specific charge capacity measured for reference cells assembled using commercial $LiNi_{1/3}Mn_{1/3}Co_{1/3}O_2$ (NMC) as cathode and lithium metal as anode from three different suppliers: lithium 1 (99.8%), lithium 2 (99.9%), and lithium 3 (99.9%). Commercial electrolyte from Solvionic (1 M $LiPF_6$ in ethylene carbonate:dimethyl carbonate, 1:1 vol%, 99.9%, H_2O < 20 ppm) was used as electrolyte and Whatman glass fiber grade GF/D was employed as separator. Coin cells 2032 were assembled and tested using the same protocol at room temperature using a Maccor 4000 series cycling at a current rate of C/10.

delivered to sustain the advent of next-generation Li-based batteries. In addition, assessment of the scalability and viability of competing Li-purification strategies toward reproducible pristine Li metal substrate are also missing, at least in the academic domain. Although integration of new processing and handling methods may require significant modifications in the existing battery production lines, the potentially significant benefits in terms of energy density, cyclability and safety justify fundamental research in the area toward a better informed evaluation of the subject.

We substantiate the criticality of the current, far from absolute, control of Li metal by considering the electrochemical performance of three different commercial Li samples. As shown in **Figure 1**, lithium samples from three different suppliers, with rather similar nominal purity (99.8%, 99.9%, and 99.9% with Na, K, Ca, and N as main contaminants always below 300 ppm) result in slightly different electrochemical behaviors. Notably, they offer three different reproducibility trends. Whereas the lithium with the lowest purity (lithium 1) leads to the highest reproducibility, 2% of the measured capacity, the other two lithium anodes tested (lithium 2 and 3) result in deviations of 3% and 7%, respectively.

The grossly limited reproducibly demonstrated in Figure 1 defines a far from ideal scenario. It illustrates exemplary the unquestionable need and urgency of improved protocols for processing of metal Li, both in terms of purification and controlled prepassivation and eventual functionalization. To this end, here we move the first steps on both accounts by first presenting a viable sputtering route to cleaning of metal Li anodes, and eventually quantifying the change of its composition and electronic properties following reaction with atmospheric gases (O_2, CO_2, and N_2). The availability of quantitatively resolved experiments on Li substrates of controlled composition enables scrutiny, and in the case of N_2 revision, of current understanding of the chemistry of metal Li in the presence of atmospheric gases. The present approach and results lay the basis for systematic and reproducible study of passivation strategies for metal Li anodes toward delivery of high energy density electrochemical storage by Li–metal, Li–S and Li–O_2 battery technologies.

2. Results and Discussion

2.1. Existing Results and Debates

The surface reactions of Li with gases have been experimentally studied since 1895.[2,3] The initial research interests were on the interaction of air and its individual component gases (O_2, CO_2, N_2, and H_2O) with Li.[4,5] These seminal studies concluded that Li metal does not react with dry N_2, O_2, or CO_2 at temperatures below 160, 250, and 300 °C, respectively. Even at high temperatures, the lithium oxidation rate appears to be very low up to its flash point (630 °C).[6] However, if moisture is present (>10 ppm of water), the reaction of Li metal with nitrogen takes place exothermically leading to the formation of a brown-reddish, sometimes defined as pink, coating of Li_3N. Analogously, for the oxygen reaction in the presence of moisture, an exothermic process will result in an oxide coating that prevents further oxidation of the lithium.[7] Finally, the reaction of CO_2 with lithium metal in presence of moisture will occur spontaneously forming lithium carbonate,[5] and the initial carbonate coating will significantly slow down further reactions.[6]

However, more recent studies contradict these earlier conclusions. All the most recent studies agree on oxidation of lithium surface by dry oxygen.[8–10] The effect of trace moisture in this reaction is believed to disrupt the passivation of Li metal.[11] We also find experimental evidence of the spontaneous reaction of lithium surface with dry CO_2 to form lithium carbonate.[12,13]

Regarding the interaction of lithium with nitrogen gas, there is still some controversy about the formation of Li_3N. Some authors consider nitrogen gas to be, together with oxygen and water, the most reactive residual gas for metallic lithium in ultrahigh vacuum systems.[14] Formation of a passivating Li_3N layer by direct chemical reaction of N_2 at room temperature and atmospheric pressure under continuous nitrogen flow has been reported in the literature.[15–17] However, in stark contrast with these results others observe either that the reaction does not take place spontaneously.[18]

Motivated by these contrasting results, the goal of the present contribution is to unravel the interactions of metallic lithium and dry atmospheric gases by monitoring the chemical changes that O_2, CO_2, and N_2 gases induce on a pure metallic lithium surface under highly reproducible conditions. The chances for lithium to be in contact with the most common dry atmospheric gases is very high, especially when working in dry rooms. According to a recent study, the changes in the ionic conductivity of freshly deposited lithium surface when interacting with surrounding gases as CO_2 and N_2 affects the

mechanism of deposition of lithium with direct consequences for the dendrite growth.[26]

2.2. Work Function as Monitoring Parameter

We chose the work function (w_f) as monitoring parameter to determine the suitability of protective layers on Li metal surfaces following preliminary DFT screening of gas-treatment methods for the stabilization of Li metal anodes,[27] and considering the importance of the work function in redox processes, electron-emitting and photoelectrochemical devices.[28–30] The chemical potential of a system of electrons at zero Kelvin is equivalent to the Fermi energy,[31] and it is often used, to approximately define the potential difference (E) of an electrochemical cell,[32,33] neglecting temperature and interfacial effects. E can be defined as the potential of the negative electrode (E_{anode}) relative to that of the positive one ($E_{cathode}$)

$$E = E_{anode} - E_{cathode} \quad (1)$$

However, as described by Trasatti,[34] access to contact potential of the electrode–electrolyte interface ($\Delta^{electrode}_{electrolyte}\psi$) and the electrode's work function (w_f) is needed for definition of the absolute electrode potential [$E_{electrode}$(abs)] for both the anode and cathode

$$E_{electrode}\,(abs) = w_f + \Delta^{electrode}_{electrolyte}\psi \quad (2)$$

For a metal in vacuum and in absence of excess surface charge, the work function (w_f) is equivalent to the position of the Fermi level with respect to vacuum.[35] It depends on the surface structure and changes in the electronic distribution across the bulk-surface–vacuum interface. Although w_f provides an incomplete description of the absolute electrode potentials, Equation (2), it is nevertheless a useful measurable observable to characterize native and processed lithium surfaces in terms of electronic properties and ensuing energy drive to electron transfer: an aspect critical to the functioning of electrochemical cells.

2.3. O_2 Gas Interaction

When lithium interacts with O_2, the expected lithium oxide on the surface is obtained. No other compound related to the oxidation is formed, not even at the highest dose of O_2 gas (1000 L in **Figure 2**). O_2 treatment results in the complete oxidation of the lithium surface after 9 L dose, as shown in **Figure 3**a. Considering the Li 1s photoelectrons kinetic energy (1197.2 eV) and the TPP2m formula from the QUASES-IMFP software version 3.0 (Quases-Tougaard), the inelastic mean free path (IMFP) for the Li 1s photoelectrons is 28.61 Å. Therefore, since the probing depth of the XPS can be estimated as three times the IMFP, the oxide layer is, at least, 85.8 Å thick. The presence of lithium oxide is also confirmed by the energy loss peak evolution around 65 eV assigned to surface excitons of Li_2O.[8,36] The evolution of the Li_2O energy loss peaks and Li^0 plasmon peaks for the low dose range can

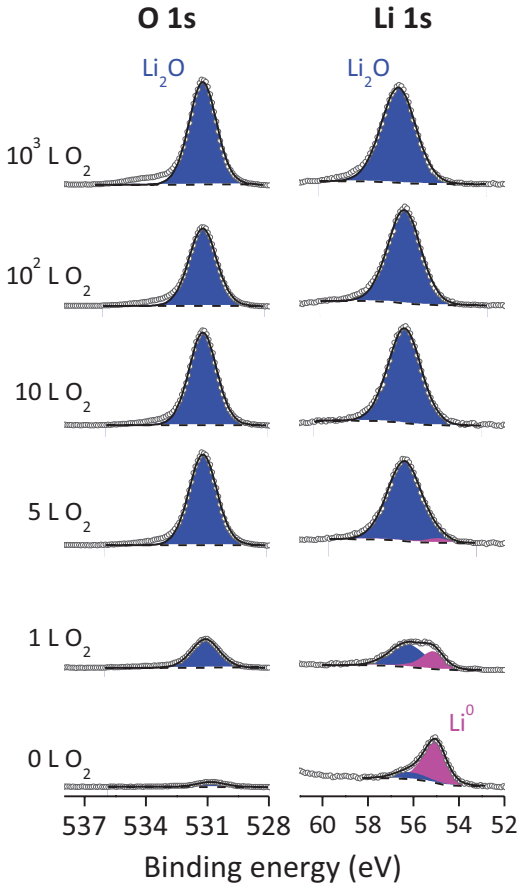

Figure 2. Experimental photoelectron peaks (open circles) measured in a clean lithium surface and exposed to different oxygen gas doses: 1 L, 5 L, and 10 L (low dose range); 100 L and 1000 L (medium dose range). The deconvolution of the O 1s and Li 1s photoelectron peaks demonstrates the evolution of Li_2O (blue components) along with the spurious presence of Li^0 (pink component) at the beginning of the experiment. The fitted curve (black line) agrees very well with experimental data, where background is represented by a dashed line.

be found in Figure S1 in the Supporting Information, where the components area can be used to estimate the O_2 dose that leads to full coverage of the Li surface by lithium oxide: around 3–4 L of O_2.

The oxidation process results in a decrease of the work function as the lithium oxide covers the Li surface (Figure 3). Such a decrease of the work function could be at a first view quite surprising, taking into consideration the electronegative nature of oxygen, which suggests an increase in the value of w_f as it has been reported elsewhere.[37] However, such an attempted interpretation is both simplistic and misleading. The observed changes in work function are due to the change in the dipole density (μ_σ) for the passivated surface, which in turn depends not only on the presence of oxide atoms (or other electron-scavenging species such as carbonate or nitride ions, vide infra), but also on the structural and electronic relaxation they induce across the vacuum-exposed passivated system.[38–40] The dipole density changes obtained from both the measured and calculated (Table S1, Supporting Information) changes in w_f indicate

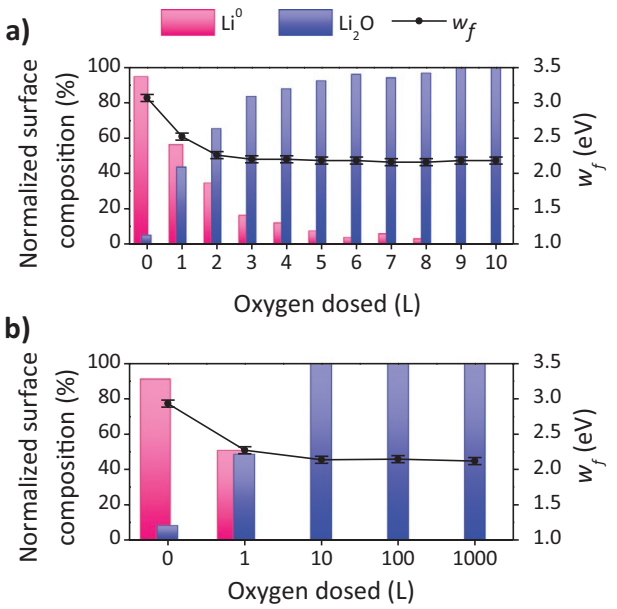

Figure 3. Normalized surface composition (left vertical axis) and work function evolution (right vertical axis) of a clean metallic lithium foil exposed to different doses of O_2: a) low dose range from 0 to 10 L and b) medium dose range from 10 to 1000 L. The lithium surface is oxidized by the gas and this results in a decrease of the work function.

that formation of subsurface Li_2O layers subtracts electronic density from the vacuum-exposed topmost surface layers, creating a positive-outward dipole density, which in turn facilitates electron extraction from the samples with respect to the bare Li surface.

A w_f decrease upon Li oxidation was reported in the 1990s by the group of Ertl.[41,42] However, there is a substantial discrepancy between the work reported 30 years ago and the present result: Ertl and coworkers observed a decrease of the w_f only until an O_2 exposure of 2 L, followed by an increase of w_f for > 2 L doses. In contrast, we observe that w_f does not increase for O_2 doses above 2 L (Figure 3). This difference could be due to either the fact that their starting clean surface could contain 10%-20% of lithium oxide or the different approach used to determine the work function; in refs. [41, 42] the authors used estimates from calculations of metastable deexcitation spectroscopy. Conversely, here we directly measure the work function.

Considering the relation of the normalized amount of Li_2O present on the Li surface and the evolution of the measured work function, an exponential correlation can be empirically established (Figure S2, Supporting Information)

$$w_f = 2.09 + 1.11e^{-0.03n} \quad (3)$$

where n is the Li_2O percentage of normalized surface composition.

When the formation of lithium oxide starts on the surface, there is a pronounced decrease of w_f, but when the oxide quantity is higher than the metallic lithium, the w_f value converges to a constant value. This indicates that the outermost layer Li_2O is the one completely dominating the electronic response of the surface, which significantly differs from Li^0 response. Another important feature of Equation (3) relies on the possibility to calculate w_f of the surface just from the lithium oxide concentration, which can be quickly determined, for example, by XPS.

As reported in the literature,[27] dissociative adsorption of 0.5 monolayer (ML) O_2 on different [(100), (110), and (111)] Li(bcc) surfaces is calculated to reduce by up to 1.2 eV the w_f value of the composite system, in qualitative agreement with the experiments in Figure 3 for dosages <3–4 L (1 ML). As DFT predicts O_2 dissociative adsorption to be energetically favored on the Li(110) surface,[27] this termination was taken as model system for the simulation of larger O_2 dosages. Following the same geometry optimization—room temperature molecular dynamics (MD)—geometry optimization screening protocol as in ref. [27] we modeled dissociative adsorption of progressively larger dosages of O_2 (0.5–1.5 ML) on Li(110).

Figure S3 in the Supporting Information reports the calculated w_f of Li(110) as a function of the modeled O_2 coverage for the optimized systems. These are shown in Figures S4–S6, and structurally analyzed in Table S2 in the Supporting Information. In semiquantitative agreement with the experimental results, adsorption of 0.5 ML on O_2 is calculated to reduce the system's w_f by roughly 0.4 V. Adsorption of additional O_2 molecules up to 1 ML leads to further reduction (1.2 V) of w_f with respect to the calculated value for the bare slab (3.2 eV). Dosage of two additional O_2 molecules on each side of the slab, for a total 1.5 ML coverage, results in barrierless dissociation of only one molecule (for each side of the slab), with the residual un-dissociated molecules leaving the substrate during the MD trajectories. Removal of the un-dissociated molecules from the simulation cell (1.25 ML coverage), followed by geometry optimization results in a w_f value of roughly 2.7 eV, i.e., 0.5 eV lower than for the bare Li(110) slab (3.2 eV). The calculated barrierless dissociation for O_2 on Li(110) for coverages between 0.25 ML[27] and 1.25 ML (but not for higher ones) corroborates interpretation of the experimental w_f plateau for dosages (coverages) larger than 3–4 L (1 ML) as being due to a lack of reactivity between the prepassivated Li surface and further incoming O_2 molecules.

Thus, in spite of the obvious limitation of the model system, starting from approximation of the Li foil as a single-crystal Li(110)-2 × 1 surface, DFT simulations semiquantitatively recover the observed trends for w_f as a function of the reaction with O_2, inviting rationalization of the physicochemical mechanisms at play, which we provide in the following.

In conjugation with previously published results for 0.5 ML O_2 on Li(110),[27] analysis of the optimized geometries and corresponding atom projected density of states (PDOS) (Figures S4–S6, Supporting Information) reveals several peculiar features. First, due to large exothermicity of the reactions (>10 eV E_{form} per dissociated O_2 molecule) successive (barrierless in our simulations) dissociation of O_2 molecule up to 1.25 ML proceeds by a mechanism whereby newly dissociated O_2 molecules push preformed oxide ions deeper in the Li slab. Bader charge analysis for the dissociated O atoms reveals rather uniform charges (–1.65/–1.81; Table S3 in the Supporting Information) regardless of their location in the passivated Li_xO layer. These results indicate the dissociated O-atom experiencing an electronically rather homogenous local environment, in line with

the negligible shift for photoelectron peaks of Li_2O as a function of O_2 dosage in Figure 2.

Although subsurface fully oxidized (into Li_2O) regions of the slab are computed to be markedly insulating (>4 eV local band-gaps), the topmost Li and O layers are calculated to be metallic, displaying a nonzero projected density of states (PDOS) at the Fermi level. The availability of metallic states (electrons) at the Fermi level sustains reaction with further incoming O_2 molecules, provided such surface states remains electronically coupled with the metallic innermost region of the slab, that in turns act as electron reservoir. Once the Li_2O layer becomes sufficiently thick to electronically decouple the metallic surface states from the bulk-like metal Li(0) electron-reservoir (1.25 ML in the simulations, 3–4 L ≈1 ML in the experiments in Figure S1 in the Supporting Information), reductive dissociation of further O_2 molecules on the prepassivated surfaces cannot proceed further as starved of the necessary electrons.

Although reported in previous DFT studies of oxidized metal Li surfaces,[27] the occurrence of metallic surface states on top of an insulating subsurface region in the passivated metal Li slabs may appear at first unexpected. However, we note that, for the clean lithium, the experimental traces of oxide present in the surface match with the binding energy of Li-rich suboxides (530.8 eV in Figure 2). This is consistent with the ion assisted process used for surface cleaning that typically results in reduction of metal oxides. As O_2 is dosed, the binding energy quickly shifts to the expected value for Li_2O, which in the literature is found in the 531.20 ± 0.06 eV range.[18] This value should remain constant as the O_2 dose increases. However, a small shift is observed with increasing O_2 dose. Although fairly small (0.05 and 0.07 eV), the energy resolution of our system (<0.05 eV) renders the measured shift significant. The observed shift to higher binding energies can be due to either i) the formation of a more oxidized species or ii) surface charging due to the presence of insulating material underneath the metallic surface region, in qualitative agreement with DFT results (Figures S4–S6). Given the challenges in defining more oxidized species than the Li_2O detected by XPS in Figure 2, argument (ii), metallic surface states on top of an insulating subsurface region, emerges as the most plausible, indirectly supporting the results of the simulations.

2.4. CO_2 Gas Interaction

In this case, besides O 1s and Li 1s, the C 1s line also appears with contributions from adventitious carbon, CO species and lithium carbonate (**Figure 4**). CO species are defined as the ones formed just by C and O atoms. A detailed explanation on the CO component definition (CO)a and (CO)b can be found in the Supporting Information.

Careful analysis of the XPS spectra corresponding to CO_2 doses up to 5 L in Figure 4 confirms, at the studied pressures, Li_2O is formed on the Li surface after 1 L dose prior to the formation of lithium carbonate. However, analysis of the Li 1s XPS spectra (Figure S9a, Supporting Information) reveals that the energy loss peaks corresponding to Li_2O are not present. This result suggests that the carbon-based compounds are growing on top of Li_2O, modifying the position of the conduction band

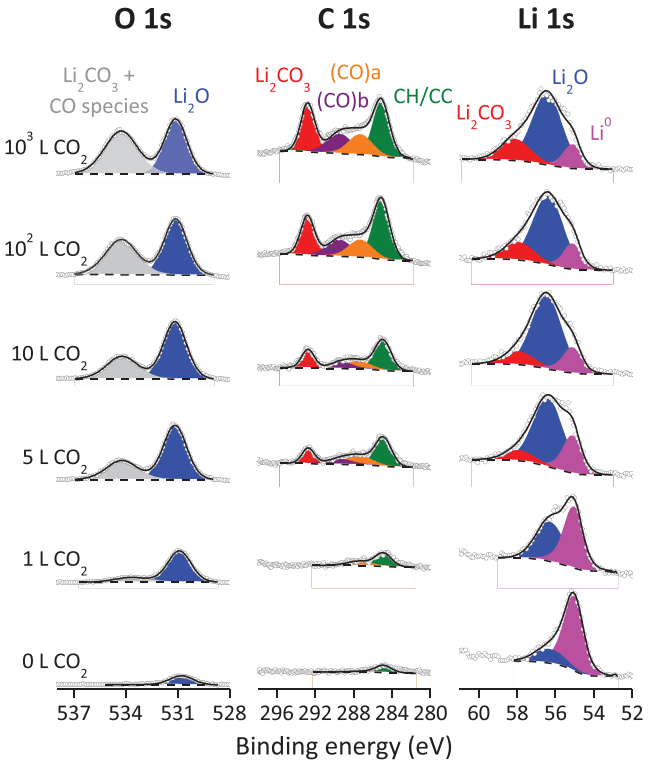

Figure 4. Experimental photoelectron peaks (open circles) measured in a clean lithium surface and exposed to different oxygen gas doses: 1 L, 5 L, and 10 L (low dose range); 100 L and 1000 L (medium dose range). The deconvolution of the C 1s, O 1s and Li 1s photoelectron peaks demonstrates the formation of Li_2O, Li_2CO_3, C-C bonds, and CO species, as well as the presence of Li^0. The fitted curve (black line) agrees very well with experimental data, where background is represented by a dashed line.

edge relative to the vacuum level and precluding the exciton formation.

We observe the oxidation of lithium metal by CO_2 to be slower than that by O_2 as metallic lithium can still be detected on the surface even after the highest CO_2 dose (1000 L in Figure 4). The CO_2 dose needed to cover all metallic lithium surface is around 8 L (Figure S9, Supporting Information). This dose is higher than for O_2 (3–4 L in Figure S1 in the Supporting Information). After 8 L of CO_2, the Li surface is covered by an overlayer of oxide and carbonates and the plasmon loss associated to Li^0 also disappears which is in agreement with having the Li metal in the subsurface region covered by an overlayer with a thickness below 10 nm. A possible explanation for the slower kinetics of the oxidation reaction is that there is a layer slowing down the lithium oxidation. Ionic conductivity of Li_2CO_3 is lower than that of Li_2O.[26] Then, considering Li ions must diffuse to the surface through the layers in order to react with the gas, the slowest oxidation could be due to the highest resistance of the ions to travel through Li_2CO_3 in comparison to Li_2O.

As for O_2, low and medium CO_2 doses cause w_f to decrease (**Figure 5**a,b). As the majority compound formed for these doses is Li_2O, it is reasonable to expect this species to be responsible for the observed decrease in w_f. Figure S10 in the Supporting Information shows that also the w_f evolution due to

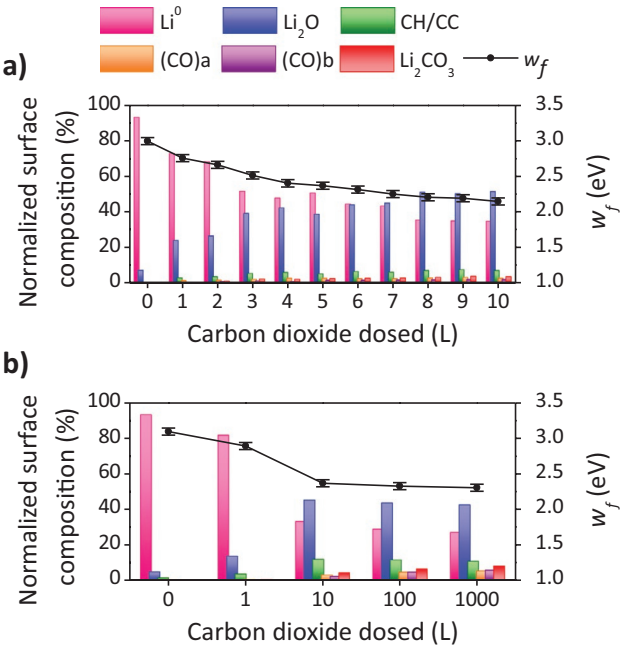

Figure 5. Normalized surface composition (left vertical axis) and work function evolution (right vertical axis) of a clean metallic lithium foil exposed to different doses of CO_2: a) low dose range from 0 to 10 L and b) medium dose range from 10 to 1000 L. In all cases, there is a remarkable presence of metallic lithium, in contrast with the surface composition after O_2 dosing. This suggests that a protective layer is formed when lithium is exposed to CO_2 gas. Analogously to the results of O_2 dosing, the work function decreases as the gas is dosed in the low dose range.

CO_2 treatment follows the same correlation obtained for oxidation of lithium by O_2 (Equation (3)). The deviations of the exponential decay of w_f for O_2- and CO_2-dosed lithium surfaces can be attributed to the effects that carbon-based compounds have on the surface, slowing down the oxidation reactions.

DFT simulation of 0.5 ML CO_2 on Li(110), first reported by Koch et al.,[27] suggest a 0.5 eV reduction of w_f with respect to the bare Li(110) substrate (Figure S3, Supporting Information). This value is in semiquantitative agreement with the measured (0.6 eV) reduction induced by 4 L (0.5 ML). The dissociative adsorption of 0.5 ML CO_2 is computed to take place via formation of acetylendiolate ($C_2O_2^{2-}$) products, accompanied by subsurface oxide-ion formation in a 1:1 ratio (1 oxide ion per C_2O_2 molecule formed).[27]

Addition of two further CO_2 molecules (1 ML coverage) on each side of the (0.5 ML CO_2) prepassivated slab invariably resulted in no CO_2 molecular or dissociative adsorption regardless of the use of geometry optimization or MD to model the systems.

We also tested whether artificial removal of the outermost Li atoms could activate dissociation of the additional CO_2 molecules and found this not to be the case. Simulation of several differently prepared models with coverages in the 0.75-1 ML range invariably led to calculated E_{form} more than 4 eV higher than for 0.5 ML CO_2/Li(110)-1 × 2, suggesting a strong energy drive against addition of extra CO_2 molecules on the (0.5 ML) passivated substrate. Based on these results, and the experimental evidence of negligible changes of w_f for CO_2 dosages larger than 8–10 L (≈1 ML), one is to conclude that the suppression of the metallic character of the topmost Li layer for 0.5 ML CO_2/Li(110)-1 × 2 (Figure 3 in ref. [27]) is effective in electronically decoupling the subsurface Li(0) electronic reservoir from incoming CO_2 molecules, thus preventing their further reduction (and ensuing changes in the system's w_f).

Although the XPS spectra in Figure 4 do not evidence formation of any acetylendiolate ($C_2O_2^{2-}$) products in the passivated surfaces, species with single C—C and C—H bonds are clearly detectable by XPS in Figure 4. At the same time, oxalate ($C_2O_4^{2-}$) formation has been previously observed by FTIR for CO_2 dosing on other alkali metal surfaces.[43] On these grounds, and especially given the occurrence of species with C—H bonds, we are to conclude that the adopted single crystal Li(110)-1 × 2 slab and the computational protocol followed to dose 100% pure CO_2 is too simplistic to quantitatively model the real samples. Real samples are evidently sensitive to the presence of UHV residuals and impurities that should be accordingly included in the simulations for quantitative results. Regardless of this limitation, the UPS and DFT evidence on w_f reduction following CO_2 decomposition on metal Li slab (Figures S3 in the Supporting Information and Figure 5) remains qualitatively unaffected.

2.5. N_2 Gas Interaction

No interaction between metallic lithium and nitrogen gas is observed for any of the studied doses. The surface composition, and consequently the work function (**Figures 6** and **7**), remain almost constant throughout exposure to N_2 doses between 1 and 1000 L. The slight variations observed in the work function (Figure 7) are related to the presence of Li_2O impurities which range from 10% in the worst case (w_f = 2.86 eV) to 5% in the best case (w_f = 3.10 eV): a 0.24 eV reduction which is in agreement with the trend displayed in Figure S2 (Supporting Information). These results validate earlier DFT observations of (defect-free) metal Li surface being surprisingly inert toward dissociative adsorption of pure N_2 into Li_3N-like compounds at room temperature,[27] in stark contrast with the calculated and observed surface chemistry for O_2 and CO_2.

Since the clean lithium metal cannot reduce the N_2 and in order to analyze the effect of lithium nitride formation on the electronic structure of lithium, a different approach based on work done by Ishitama et al.,[44] was used to obtain Li_3N: reactive ion implantation. This method allowed to prepare a surface mainly composed by lithium metal and lithium nitride (**Figure 8**) as determined by XPS analysis of Li 1s, O 1s, and N 1s, where the normalized surface composition was 68.4% Li^0, 19.8 Li_3N, 8.1% Li_2O, and 3.7% of a small amount of impurity that we called N1.

The formation of Li_3N leads to a change on the w_f value as determined by UPS, from 3.01 eV of Li^0 to 2.49 eV in the Li_3N-containing surface. Considering that the final surface also contains 8.1% of Li_2O, one could think that the w_f decrease is due to lithium oxide formation. However, according to the correlation obtained for O_2 and CO_2 dosing, Equation (3), such amount of surface Li_2O should result in w_f = 2.97 eV, far above the 2.49 eV measured. So, lithium nitride formation also reduces the work

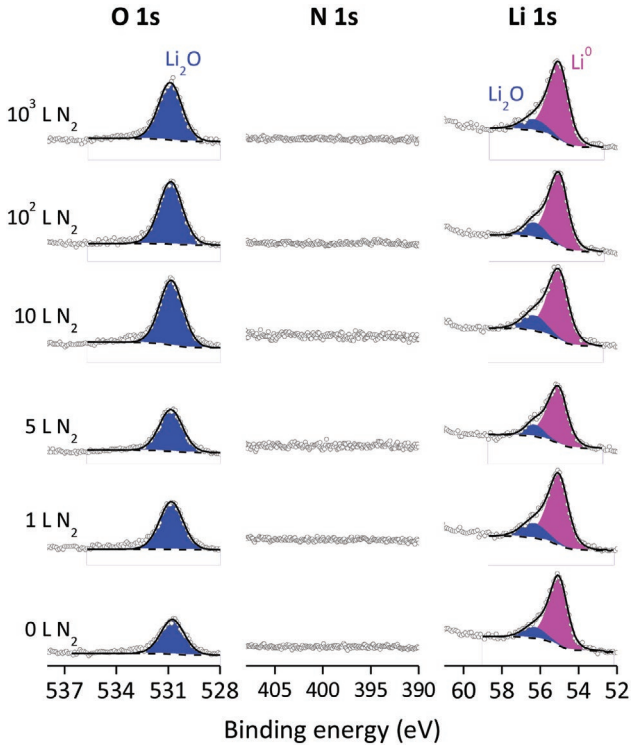

Figure 6. Experimental photoelectron peaks (open circles) measured in a clean lithium surface and exposed to different nitrogen gas doses: 1 L, 5 L, and 10 L (low dose range); 100 L and 1000 L (medium dose range). The deconvolution of the N 1s, O 1s and Li 1s photoelectron peaks demonstrates the existence of Li_2O only, as well as the dominating presence of Li^0. The fitted curve (black line) agrees very well with experimental data, where background is represented by a dashed line.

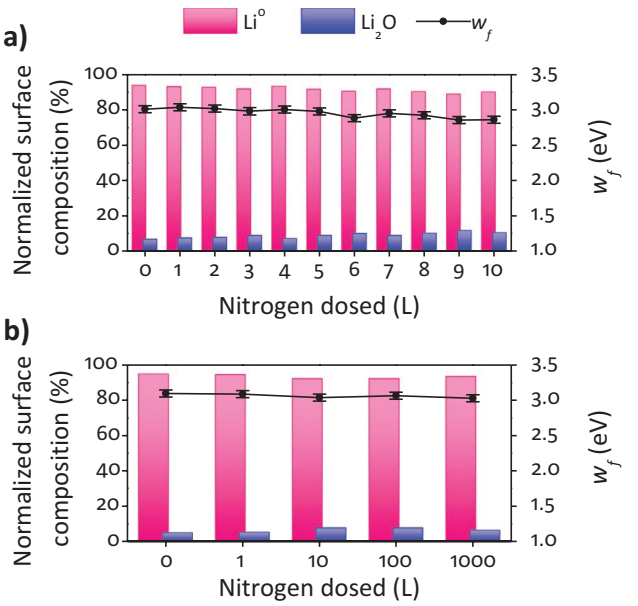

Figure 7. Normalized surface composition (left vertical axis) and work function evolution (right vertical axis) of a clean metallic lithium foil exposed to different doses of N_2: a) low dose range from 0 to 10 L and b) medium dose range from 10 to 1000 L. In all cases, there is a dominating presence of metallic lithium, highlighting the absence of reaction between lithium and nitrogen gas. In contrast with observations for other gases, the work function remains constant throughout the experiment.

function of the lithium metal. This conclusion get strengthen by the calculated w_f (2.5 eV) for the energetically favored structure of 0.5 ML N adatoms on Li(110), in the presence of ≈2.7 electron transfer to the N atoms.[27]

As mentioned in the introduction, there are several studies where Li_3N is obtained just by direct reaction between lithium and nitrogen gas.[15–17] All these studies, however, use atmospheric pressures. Considering how sensitive is lithium to both oxygen and carbon dioxide gases, even pressures of 1×10^{-8} mbar modify the surface, it is be reasonable assuming that studies at atmospheric pressure are conditioned by the traces of impurities that will have a major impact on the surface reactions of the starting surface hence determining the evolution of the surface compounds. In other words, metallic lithium surface, out of UHV conditions, is going to have a significant contamination overlayer even if exposed to pure gases. Then, the formation of Li_3N observed in other works could be related to the surface impurities of lithium that catalyze the lithium nitride formation.

3. Conclusions

Combined DFT studies with experimental XPS and UPS measurements on O_2, CO_2, and N_2 treatment of metal lithium surfaces demonstrates that each of the considered gases has a singularity when interacting with clean metallic lithium. Oxygen leads to a dramatic oxidation of the surface with complete removal of metallic lithium from the topmost 8.5 nm of the surface after 9 L O_2. Lithium oxidation by carbon dioxide is slower than by oxygen due to the creation of less-reactive carbon-based compounds on the surface. These two gases decrease the work function of the surface in the ranges of 1 to 1000 L doses. Experimentally, we establish an exponential decay of the work function for passivated Li metal as a consequence of the increase of Li_2O at the surface (Equation (3)). XPS and UPS measurements demonstrate unambiguously that there is no reaction between metallic lithium and nitrogen gas for the studied pressures. In our studies, the only way to obtain

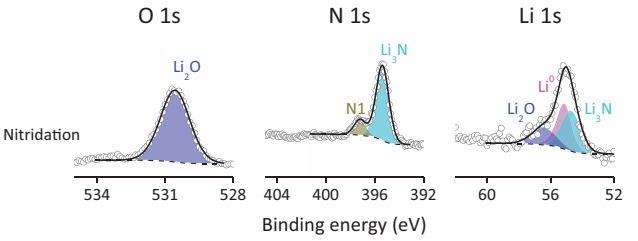

Figure 8. Experimental photoelectron peaks (open circles) measured on the lithium surface after nitrogen ion implantation. The deconvolution of the N 1s, O 1s, and Li 1s photoelectron peaks demonstrates the presence of Li_2O and Li^0, only after bombarding the sample with nitrogen ions, the lithium nitride is formed on the surface. This process leads to a decrease on the work function. The fitted curve (black line) agrees very well with experimental data, where background is represented by a dashed line.

lithium nitride is by reactive ion implantation. This Li_3N layer also decreases the work function of the surface.

For metallic lithium to be implemented as anode in Li-based batteries, there must be a solid electrolyte interface able to maintain a uniform surface after long cycling period. Ideally, this surface needs to be ionically conductive but electronically insulating, with reduced propensity to reduce interacting electrolyte molecules. In this study we obtain lithium surfaces with the opposite electronic properties. The observed decrease of the work function indicates increase of the Fermi energy relative to the vacuum level, with an inevitably enhanced energy drive for the treated surface to lose electrons and reduce interacting species. Therefore, we find O_2 and CO_2 gas treatment, as well as nitrogen ion implantation, to be detrimental for the electronic properties of metal lithium anodes.

4. Experimental Section

Surface Characterization: The techniques that were chosen to study the effect O_2, CO_2, and N_2 gases produce on the lithium surface are X-ray photoelectron spectroscopy (XPS) and ultraviolet photoelectron spectroscopy (UPS). The first one is used to determine the different compounds present on the Li surface. The second surface characterization technique provides information about the valence band and it is also used to record the work function evolution of the surface.

Both spectroscopies (XPS and UPS) were carried out in the multitechnique surface analysis system available at CIC energiGUNE. This consists of a set of interconnected ultrahigh vacuum (UHV) chambers with a base pressure of 1×10^{-10} mbar equipped with different surface analysis techniques and surface preparation methods. XPS measurements were performed with a Phoibos 150 SPECS spectrometer having an energy resolution better than 2 meV and using a non-monochromatic X-ray source. The measurements were recorded with the analyzer in Fixed Analyzer Transmission mode and a Mg Kα photon source ($h\nu = 1253.6$ eV) with a power of 100 W. The pass energy was set to 90 eV for survey spectra acquisition and 40 eV for the detailed regions of each element. All XPS data processing was carried out using CasaXPS version 2.3.19PR1.0 (Casa Software Ltd, Teighmouth, UK). Specification about XPS data treatment, calibration and quantification are detailed in the Supporting Information. References and constrains used to identify the surface compounds can be found in Table S5 in the Supporting Information. UPS spectra were taken with a He I emission lamp ($h\nu = 21.2$ eV) and the same photoelectron analyzer set to low angular dispersion mode for Fermi edge determination or to standard transmission mode for all other UPS acquisitions. Information about how to obtain the work function from UPS spectra is described in Figure S11 in the Supporting Information.

Surface Modification: Commercial lithium foil (Rockwood Lithium, lithium metal, battery grade, 99.8%) was stored in argon atmosphere in a glove box (MBRAUN) where O_2 and H_2O levels were below 0.1 ppm. After being mounted in the sample holders, the foils were transported to the UHV system with a specific transfer tool, which allows the transportation of the sample either in vacuum or in argon atmosphere. Once in the UHV system, Ar^+ ion sputtering at 5 keV was performed using a SPECS IQE 12/38 ion source to remove the surface layer from the Li foil; an extensively reported method to clean oxides from metal surfaces.[18,45] This ion source has a differential pumping stage that allows operation at 10^{-7} mbar of Ar. The sputter cleaning method has been reported to deliver the same fresh Li surfaces as in situ fracture.[46] Once the lithium's native overlayer was removed, a clear signal corresponding to Li° could be observed with XPS (Figure S12, Supporting Information). The various gas exposures of the samples were carried out in the preparation chamber of the UHV system (base pressure of 1×10^{-10} mbar), which is equipped with a high precision leak valve to control the dose of each gas.

O_2 (Praxair, 99.9% purity), CO_2 (Laborgase, 99.995% purity), and N_2 (Praxair, 99.9% purity) were measured in two dose ranges: 1–2–3–4–5–6–7–8–9–10 L as low dose range and 1–10–100–1000 L as medium dose range. L (Langmuir) unit corresponds to a dose of 10^{-6} Torr of a given gas during one second. The specific pressures used in each dose are detailed in Table S6 in the Supporting Information. Every dosing sequence was deployed starting from a UHV cleaned lithium. As it will be discussed later, the interaction of metallic lithium and nitrogen required the ion implantation of nitrogen ions by means of a SPECS IQE 11/35 ion source operated at 0.5 keV under an Ar partial pressure of 10^{-5} mbar, being the base pressure of the system 10^{-10} mbar.

Computational Details: Density functional theory (DFT) simulations were performed via the projected augmented wave (PAW) method as implemented in the VASP program.[47] In all cases, the PBE exchange-correlation (XC) functional, a 400 eV plane wave energy cutoff, and 0.2 eV Gaussian smearing were used.[48] The vacuum buffer along the nonperiodic direction of the slab models was at least 15 Å. Following earlier tests on the negligible effects of van der Waals corrections on the dissociative adsorption of the systems of interest,[27] they were not applied in the simulations.

To prevent the introduction of artificial dipoles perpendicular to the surfaces, molecules were symmetrically adsorbed on both sides of the slab. The position of all the atoms in the models were relaxed maintaining the initial symmetry plane of the slab via the RMM-DIIS quasi-Newton algorithm, and using a force-convergence threshold of 0.05 eV $Å^{-1}$.[49]

Available DFT results on adsorption of (1 monolayer, ML) CO_2, O_2 and N_2 on metallic Li surfaces, indicate that these gases adsorb preferentially on the Li(110) surface.[27] We accordingly focused on this substrate for the simulation of 0.5–1.25 ML coverages. Following ref. [27], an (orthorhombic) Li(110)-2 × 1 simulation cell (four Li atoms on each side of the slab) was constructed using the DFT-optimized lattice constant for bulk bcc Li: 3.466 Å. For all cases, we used $7 \times 10 \times 1$ grids of symmetry-irreducible *k*-points, previously checked to yield energies converged to within less than 1 meV per atom.[27]

Modeling of CO_2 adsorption was carried out using a 13 Li-layer slab. Conversely, and due to the increased reactivity of Li surfaces toward O_2, simulations for these systems were carried out using a thicker 25 Li-layer slab, numerically checked to maintain bulk-like density of states (DOS) and Bader charges in its innermost region.

Given their use for equilibration-only purposes, canonical (NVT) molecular dynamics (MD) simulations were run using the Verlet integration algorithm and the Berendsen thermostat as implemented in VASP.[50,51] In all cases, the time step was 1.5 fs. Geometry optimization and MD runs for all the molecularly decorated slabs were carried out allowing unconstrained spin-polarization in the system.

Bader charge analyses were carried out on the basis of the total charge density, i.e., accounting for both the electronic and ionic core charges. Slab formation energies (E_{form}) were calculated as:[52]

$$E_{form} = E_{slab} - N_{Li}E_{Li-bulk} - N_{mol}E_{mol} \quad (4)$$

where N_{mol} is the number of gas molecules initially present in the system and E_{mol} is the energy of one molecule optimized in vacuo.

Work functions (w_f) were calculated from the difference between the vacuum-electrostatic plateau (E_v) in the (periodic) simulation cell and the computed Fermi energy (E_F)

$$w_f = E_v - E_F \quad (5)$$

Equation (5) includes by construction the shift in E_v due electrostatic dipole densities at the surface arising from structural and electronic relaxation or transfer across the vacuum-exposed composite interface. Following refs. [40, 53], within a plane condenser model the relationship between change in work function (Δw_f) and interface dipole density ($\Delta\mu_\sigma$) can be written (in atomic units) as

$$\Delta w_f = -4\pi\Delta\mu_\sigma \quad (6)$$

For the sign-convention used, negative (positive) Δw_f ($\Delta\mu_\sigma$) values correspond to a dipole density with the positive side facing the vacuum, which facilitates electron extraction from the sample.

Supporting Information

Supporting Information is available from the Wiley Online Library or from the author.

Acknowledgements

Support from the EU FP7 program SIRBATT (contract No. 608502) is gratefully acknowledged. A.E. thanks the Basque Government for her Ph.D. fellowship. G.T. also acknowledges support from EPSRC UK (EP/I004483 and EP/K036408). This work made use of the ARCHER (via the UKCP Consortium, EPSRC UK EP/P022189/2), UK Materials and Molecular Modelling Hub (EPSRC UK EP/P020194/1), and STFC Scientific Computing Department's SCARF High-Performance Computing facilities as well as the computational resource bwUniCluster funded by the Ministry of Science, Research and the Arts Baden-Württemberg and the Universities of the State of Baden-Württemberg, Germany, within the framework program bwHPC.

Conflict of Interest

The authors declare no conflict of interest.

Keywords

lithium metal anodes, lithium anode processing, lithium-ion batteries

Received: February 9, 2020
Revised: March 31, 2020
Published online: May 4, 2020

[1] G. Li, Z. Liu, Q. Huang, Y. Gao, M. Regula, D. Wang, L. Q. Chen, D. Wang, *Nat. Energy* **2018**, *3*, 1076.
[2] M. Guntz, *C. R. Hebd. Seances Acad. Sci.* **1895**, *120*, 777.
[3] H. Deslandres, *C. R. Hebd. Seances Acad. Sci.* **1895**, *121*, 886.
[4] M. M. Markowitz, D. A. Boryta, *J. Chem. Eng. Data* **1962**, *7*, 586.
[5] J. O. Cowles, A. D. Pasternak, *Reactor Technology*, USAEC Report UCRL-50647, **1969**, https://www.osti.gov/biblio/4168308-lithium-properties-related-use-nuclear-reactor-coolant (accessed: February 2020).
[6] D. W. Jeppson, J. L. Ballif, W. W. Yuan, B. E. Chou, *HEDL-TME* Report 78-15, UV-20, **1978**, https://www.osti.gov/biblio/6885395-lithium-literature-review-lithium-properties-interactions (accessed: February 2020).
[7] C. C. Addison, B. M. Davies, *J. Chem. Soc. A* **1969**, 1822, https://pubs.rsc.org/en/content/articlelanding/1969/J1/j19690001822#!divAbstract.
[8] K. R. Zavadil, N. R. Armstrong, *Surf. Sci.* **1990**, *230*, 47.
[9] K. Wang, P. N. RossJr., F. Kong, F. McLarnon, *J. Electrochem. Soc.* **1996**, *143*, 422.
[10] S. M. Wulfsberg, B. E. Koel, S. L. Bernasek, *Surf. Sci.* **2016**, *652*, 222.
[11] Y. Li, Y. Li, Y. Sun, B. Butz, K. Yan, A. L. Koh, J. Zhao, A. Pei, Y. Cui, *Nano Lett.* **2017**, *17*, 5171.
[12] H. Gan, E. S. Takeuchi, *J. Power Sources* **1996**, *62*, 45.
[13] G. Zhuang, Y. Chen, P. N. Ross, *Surf. Sci.* **1998**, *418*, 139.
[14] W. Mclean, J. A. Schultz, L. G. Pedersen, R. C. Jarnagin, *Surf. Sci.* **1979**, *83*, 354.
[15] M. Wu, Z. Wen, Y. Liu, X. Wang, L. Huang, *J. Power Sources* **2011**, *196*, 8091.
[16] G. Ma, Z. Wen, M. Wu, C. Shen, Q. Wang, J. Jin, X. Wu, *Chem. Commun.* **2014**, *50*, 14209.
[17] Y. J. Zhang, W. Wang, H. Tang, W. Q. Bai, X. Ge, X. L. Wang, C. D. Gu, J. P. Tu, *J. Power Sources* **2015**, *277*, 304.
[18] K. N. Wood, G. Teeter, *ACS Appl. Energy Mater.* **2018**, *1*, 4493.
[19] J. Qian, W. A. Henderson, W. Xu, P. Bhattacharya, M. Engelhard, O. Borodin, J.-G. Zhang, *Nat. Commun.* **2015**, *6*, 6362.
[20] M. S. Park, S. B. Ma, D. J. Lee, D. Im, S.-G. Doo, O. Yamamoto, *Sci. Rep.* **2015**, *4*, 3815.
[21] M.-H. Ryou, Y. M. Lee, Y. Lee, M. Winter, P. Bieker, *Adv. Funct. Mater.* **2015**, *25*, 834.
[22] M. S. Kim, J.-H. Ryu, Deepika, Y. R. L , I. W. Nah, K.-R. Lee, L. A. Archer, W. I. Cho, *Nat. Energy* **2018**, *3*, 889.
[23] Y. Gao, Z. Yan, J. L. Gray, X. He, D. Wang, T. Chen, Q. Huang, Y. C. Li, H. Wang, S. H. Kim, T. E. Mallouk, D. Wang, *Nat. Mater.* **2019**, *18*, 384.
[24] R. Xu, X.-B. Cheng, C. Yan, X.-Q. Zhang, Y. Xiao, C.-Z. Zhao, J.-Q. Huang, Q. Zhang, *Matter* **2019**, *1*, 317.
[25] Y. Zhu, X. He, Y. Mo, *Adv. Sci.* **2017**, *4*, 1600517.
[26] Y. He, X. Ren, Y. Xu, M. H. Engelhard, X. Li, J. Xiao, J. Liu, J.-G. Zhang, W. Xu, C. Wang, *Nat. Nanotechnol.* **2019**, *14*, 1042.
[27] S. L. Koch, B. J. Morgan, S. Passerini, G. Teobaldi, *J. Power Sources* **2015**, *296*, 150.
[28] H. B. Michaelson, *J. Appl. Phys.* **1977**, *48*, 4729.
[29] P. Bergveld, J. Hendrikse, W. Olthuis, *Meas. Sci. Technol.* **1998**, *9*, 1801.
[30] M. Grätzel, *Nature* **2001**, *414*, 338.
[31] C. Kittel, H. Kromer, *Thermal Physics*, 2nd ed., W. H. Freeman, New York **1980**.
[32] J. Gao, S.-Q. Shi, H. Li, *Chin. Phys. B* **2016**, *25*, 018210.
[33] J. B. Goodenough, K.-S. Park, *J. Am. Chem. Soc.* **2013**, *135*, 1167.
[34] S. Trasatti, *J. Electroanal. Chem.* **1986**, *209*, 417.
[35] H. Gerischer, W. Ekardt, *Appl. Phys. Lett.* **1983**, *43*, 393.
[36] L. Liu, V. E. Henrich, *Phys. Rev. B* **1996**, *54*, 2236.
[37] D. Ensling, A. Thissen, W. Jaegermann, *Appl. Surf. Sci.* **2008**, *255*, 2517.
[38] R. Smoluchowski, *Phys. Rev.* **1941**, *60*, 661.
[39] G. E. Rhead, *Appl. Surf. Sci.* **1991**, *47*, 35.
[40] J. Junquera, M. H. Cohen, K. M. Rab, *J. Phys.: Condens. Matter* **2007**, *19*, 213203.
[41] T. Greber, K. Freihube, R. Grobecker, A. Böttcher, K. Hermann, G. Ertl, D. Fick, *Phys. Rev. B* **1994**, *50*, 8755.
[42] K. Hermann, K. Freihube, T. Greber, A. Bröttcher, R. Grobecker, D. Fick, G. Ertl, *Surf. Sci.* **1994**, *313*, L806.
[43] O. Axelsson, Y. Shao, J. Paul, F. M. Hoffmann, *J. Phys. Chem.* **1995**, *99*, 7028.
[44] S. Ishitama, Y. Baba, R. Fujii, M. Nakamura, *JPS Conf. Proc.* **2014**, *1*, 012035.
[45] E. Taglauer, *Appl. Phys. A: Solids Surf.* **1990**, *51*, 238.
[46] S. Oswald, *Appl. Surf. Sci.* **2015**, *351*, 492.
[47] G. Kresse, J. Furthmüller, *Phys. Rev. B* **1996**, *54*, 11169.
[48] J. P. Perdew, K. Burke, M. Ernzerhof, *Phys. Rev. Lett.* **1996**, *77*, 3865.
[49] P. Pulay, *Chem. Phys. Lett.* **1980**, *73*, 393.
[50] L. Verlet, *Phys. Rev.* **1967**, *159*, 98.
[51] H. J. C. Berendsen, J. P. M. Postma, W. F. van Gunsteren, A. DiNola, J. R. Haak, *J. Chem. Phys.* **1984**, *81*, 3684.
[52] G. Henkelman, A. Arnaldsson, H. Jónsson, *Comput. Mater. Sci.* **2006**, *36*, 354.
[53] G. Teobaldi, K. Lämmle, T. Trevethan, M. Watkins, A. Schwarz, R. Wiesendanger, A. L. Shluger, *Phys. Rev. Lett.* **2011**, *106*, 216102.